

Identification of parameters of vehicles moving on bridges

L. Deng, C.S. Cai*

Department of Civil and Environmental Engineering, Louisiana State University, Baton Rouge, LA 70803, United States

ARTICLE INFO

Article history:

Received 26 May 2008

Received in revised form

22 December 2008

Accepted 3 June 2009

Available online 9 July 2009

Keywords:

Vehicle–bridge coupling system

Bridge

Vehicle

Deflection

Strain

Vibration

Influence surface

ABSTRACT

This paper presents a method for identifying the parameters of vehicles moving on bridges. Two vehicle models, a single-degree-of-freedom model and a full-scale vehicle model, are used. The vehicle–bridge coupling equations are established by combining the equations of motion of both the bridge and the vehicle using the displacement relationship and the interaction force relationship at the contact point. Bridge responses including displacement, acceleration, and strain are used in the identification process. The parameters of vehicles moving on the bridge are then identified by optimizing an objective function, which is built up using the residual between the measured response time history and predicted response time history using the Genetic Algorithm. A series of case studies have been carried out and the identified results demonstrate that the proposed method is able to identify vehicle parameters very accurately. Field tests have also been performed on an existing bridge in Louisiana, and the parameters of a real truck are predicted. Since it is able to identify the parameters of moving vehicles, the methodology can be applied to improve the current weigh-in-motion techniques that usually require a smooth road surface and slow vehicle movement to minimize the dynamic effects. The methodology can also be implemented in routine traffic monitoring and control.

© 2009 Elsevier Ltd. All rights reserved.

1. Introduction

In the past few decades, the problem of bridge vibration under moving forces or vehicle loads has been studied extensively. The dynamic performance of bridges can be affected by many factors. Different types of vehicles, vehicle speeds, and road surface conditions could all contribute to different bridge dynamic performances. For given structural properties of a bridge and road surface condition, the mechanical properties (or dynamic characteristics) of the vehicles traveling on the bridge would play a very important role in affecting the dynamic performance of the bridge. Therefore, it would be very beneficial to be able to identify the parameters of vehicles traveling on bridges.

In the literature many vehicle–bridge interaction models have been proposed for the purpose of identifying vehicle parameters. Bridges are usually modeled as simply support beams [1–3] or multi-span continuous beams [4,5]. For the vehicle model, most researchers used a single-degree-of-freedom (SDOF) system or two-DOF system [6–8], while others used a more complex twelve-parameter vehicle model [9].

Different methods for identifying vehicle parameters have been proposed in the literature [10,11,6,7,9]. Jiang et al. and Au et al. [7,6] used a genetic algorithm (GA) to identify the

parameters of vehicles traveling on a continuous bridge by minimizing the residuals between the measured accelerations and the reconstructed accelerations from the identified parameters. In their study the vehicle was modeled using either a four-parameter model with one DOF or a five-parameter model with two DOFs. For the bridge model, the modified beam functions proposed by Zheng [12] were used. Law et al. [9] presented a parameter identification method based on the dynamic response sensitivity analysis. The modified beam functions [12] were also used for the bridge, and a twelve-parameter vehicle model was used for the vehicle. The identification was realized based on the least-squares method with regularization from the measured strain, velocity, or acceleration.

In most previous works the bridge was modeled as a line beam (or one-dimensional beam). As a result, the vehicle model was usually limited to a SDOF system or two-DOF system. All the beam-model-based methodologies would become impractical if the entire bridge system is to be modeled for applications. Moreover, the over-simplified vehicle models may not be able to represent well the real vehicles traveling on bridges.

This paper presents a methodology for identifying the parameters of vehicles moving on complex bridges using the GA. Both the SDOF vehicle model and full-scale vehicle model have been used for the vehicles. A series of case studies have been carried out, and the identified results yield very good accuracy. This method has also been applied to identify the parameters of a real truck moving on an existing bridge, and the identified vehicle parameters are compared to the true parameters.

* Corresponding author.

E-mail address: CSCAI@LSU.edu (C.S. Cai).

2. Vehicle–bridge coupled system

2.1. Vehicle model

A review of different vehicle models used in the literature can be found in [13]. In the present study, two different vehicle models were used. The first model is a SDOF system consisting of a mass, spring, and damper (Fig. 1(a)). The SDOF system proved adequate to simulate the interaction between a single wheel (or vehicle) and the bridge deck [14–16]. The second model shown in Fig. 1(b) is a full-scale vehicle model, which is a combination of a rigid body connected to four masses by a series of springs and damping devices. The rigid body represents the vehicle body, the four masses represent the masses of tires and suspension systems, and the linear elastic springs and dashpots represent the tires and suspension systems [18,17]. For both models, the contact between the vehicle and the bridge deck is assumed to be a point contact. This point contact assumption has been commonly used in the literature and has been demonstrated to be able to reasonably represent the real vehicle tire system with the use of a spring and a damper [18]. However, it is cautioned that the “point contact” assumption may overestimate the excitation of the high-frequency components of the road roughness. The effect of the point contact assumption will be investigated in a future study by developing more realistic contact conditions.

For demonstration purposes, the SDOF vehicle model has been used here to establish the equation of motion of the vehicle as well as the vehicle–bridge coupling equations. A similar approach can be used for the full-scale vehicle model. The equation of motion of a SDOF vehicle can be written as below according to Newton's Second Law:

$$M_v \cdot \ddot{d}_v = -F_G + F_{v-b} \quad (1)$$

where M_v is the mass of the vehicle; \ddot{d}_v is the acceleration of the vehicle in the vertical direction; F_G is the gravity force of the vehicle; and F_{v-b} is the interaction force between the vehicle and bridge deck, which can be calculated as:

$$F_{v-b} = -K_v \cdot \Delta_L - C_v \dot{\Delta}_L \quad (2)$$

where K_v and C_v are the coefficients of the vehicle spring and damper and Δ_L is the deformation of the vehicle spring.

For the case when N vehicles are traveling on a bridge at the same time, the equations of motion for the N vehicles can be written in a matrix form as:

$$[M_v^N] \{\ddot{d}_v\} = -\{F_G^N\} + \{F_{v-b}^N\} \quad (3)$$

where $[M_v^N]$ is the diagonal mass matrix for N vehicles; $\{\ddot{d}_v\}$ is the acceleration vector in the vertical direction for N vehicles; and $\{F_G^N\}$ and $\{F_{v-b}^N\}$ are the gravity force vector and the interaction force vector for N vehicles, respectively.

2.2. Bridge model

The equation of motion for a bridge can be written as follows:

$$[M_b] \{\ddot{d}_b\} + [C_b] \{\dot{d}_b\} + [K_b] \{d_b\} = \{F_b\} \quad (4)$$

where $[M_b]$, $[C_b]$, and $[K_b]$ are the mass, damping, and stiffness matrices of the bridge, respectively; $\{d_b\}$ is the displacement vector for all DOFs of the bridge; $\{\dot{d}_b\}$ and $\{\ddot{d}_b\}$ are the first and second derivative of $\{d_b\}$ with respect to time, respectively; and $\{F_b\}$ is a vector containing all external forces acting on the bridge.

With the modal superposition technique, the displacement vector of the bridge $\{d_b\}$ in Eq. (4) can be expressed as:

$$\{d_b\} = [\{\Phi_1\} \ \{\Phi_2\} \ \dots \ \{\Phi_m\}] \{\xi_1 \ \xi_2 \ \dots \ \xi_m\}^T = [\Phi_b] \{\xi_b\} \quad (5)$$

where m is the total number of modes used for the bridge

under consideration; $\{\Phi_i\}$ and ξ_i are the i th mode shape of the bridge and the i th generalized modal coordinate, respectively. Each mode shape is normalized such that $\{\Phi_i\}^T [M_b] \{\Phi_i\} = 1$ and $\{\Phi_i\}^T [K_b] \{\Phi_i\} = \omega_i^2$. Accordingly, $\{\dot{d}_b\}$ and $\{\ddot{d}_b\}$ can also be expressed using the mode shapes and the generalized modal coordinates as follows:

$$\begin{aligned} \{\dot{d}_b\} &= [\{\Phi_1\} \ \{\Phi_2\} \ \dots \ \{\Phi_m\}] \{\dot{\xi}_1 \ \dot{\xi}_2 \ \dots \ \dot{\xi}_m\}^T \\ &= [\Phi_b] \{\dot{\xi}_b\} \end{aligned} \quad (6)$$

$$\begin{aligned} \{\ddot{d}_b\} &= [\{\Phi_1\} \ \{\Phi_2\} \ \dots \ \{\Phi_m\}] \{\ddot{\xi}_1 \ \ddot{\xi}_2 \ \dots \ \ddot{\xi}_m\}^T \\ &= [\Phi_b] \{\ddot{\xi}_b\} \end{aligned} \quad (7)$$

In this study the damping matrix $[C_b]$ in Eq. (4) is assumed to be equal to $2\omega_i \eta_i [M_b]$, where η_i is the percentage of the critical damping for the i th mode of the bridge. Eq. (4) can now be rewritten as:

$$[I] \{\ddot{\xi}_b\} + [2\omega_i \eta_i I] \{\dot{\xi}_b\} + [\omega_i^2 I] \{\xi_b\} = [\Phi_b]^T \{F_b\} \quad (8)$$

where $[I]$ = unit matrix.

2.3. Road surface condition

The road surface condition is an important factor that affects the dynamic responses of both the bridge and vehicles. A road surface profile is usually assumed to be a zero-mean stationary Gaussian random process and can be generated through an inverse Fourier transformation based on a power spectral density (PSD) function [19] as:

$$r(X) = \sum_{k=1}^N \sqrt{2\varphi(n_k) \Delta n} \cos(2\pi n_k X + \theta_k) \quad (9)$$

where θ_k is the random phase angle uniformly distributed from 0 to 2π ; $\varphi(\cdot)$ is the PSD function (m^3/cycle) for the road surface elevation; and n_k is the wave number (cycle/m). In the present study, the following PSD function [20] has been used:

$$\varphi(n) = \varphi(n_0) \left(\frac{n}{n_0}\right)^{-2} \quad (n_1 < n < n_2) \quad (10)$$

where n is the spatial frequency (cycle/m); n_0 is the discontinuity frequency of $1/2\pi$ (cycle/m); $\varphi(n_0)$ is the roughness coefficient (m^3/cycle) whose value is chosen depending on the road condition; and n_1 and n_2 are the lower and upper cut-off frequencies, respectively.

The International Organization for Standardization [21] has proposed a road roughness classification index from A (very good) to H (very poor) according to different values of $\varphi(n_0)$. In this paper the classification of road roughness based on [21] is used.

2.3.1. Assembling the vehicle–bridge coupled system

Vehicles traveling on a bridge are connected to the bridge via contact points. The interaction forces acting on the bridge $\{F_{b-v}\}$ and on the vehicles $\{F_{v-b}\}$ are actually action and reaction forces existing at the contact points. In terms of finite element modeling, these interaction forces may not apply right at any node. Therefore, the interaction forces need to be transformed into equivalent nodal forces $\{F_b^{eq}\}$ in the finite element analysis. This can be done using the virtual work principle, which states that the work done by the equivalent nodal forces and the actual force should be equal, which can be expressed as:

$$\{d_{b_nodal}\}^T \{F_b^{eq}\} = d_{contact} \cdot F \quad (11)$$

where $\{d_{b_nodal}\}$ is the displacement vector for all the nodes of the element in contact; $d_{contact}$ is the displacement of the element at

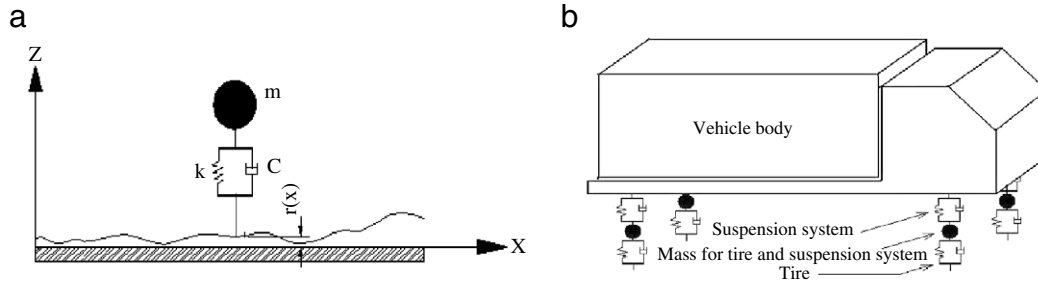


Fig. 1. Vehicle models used in the present study: (a) A SDOF vehicle model; (b) A full-scale two-axle vehicle model.

the contact point; $\{F^{eq}\}$ is the equivalent force vector applied at all the nodes of the element in contact; and F is the real force acting at the contact point.

Since $d_{contact}$ can be expressed using the displacement at each node of the element as below:

$$d_{contact} = [N_e] \{d_{b_nodal}\} \quad (12)$$

where $[N_e]$ is the shape function of the element in contact. From Eqs. (11) and (12) the following relationship between the equivalent nodal forces and the interaction force acting on the element in contact can be easily obtained:

$$\{F^{eq}\} = [N_e]^T \cdot F \quad (13)$$

To be consistent with the size of the force vector in the analysis of the full bridge, Eq. (13) can be expanded to a full force vector form as below:

$$\{F_b^{eq}\} = [N_b]^T \cdot F \quad (14)$$

where $\{F_b^{eq}\}$ is a vector with the number of elements equal to the total number of DOFs of the bridge model. It is constructed by inserting the elements in the original force vector $\{F^{eq}\}$ in Eq. (13) into their corresponding DOFs in the full force vector $\{F_b^{eq}\}$ and adding zero terms to the remaining elements in $\{F_b^{eq}\}$. For convenience, $[N_b]$ is named the shape function of the bridge. For two interaction forces acting upon different elements of the same bridge, the shape function of the bridge $[N_b]$ for the two forces would be different though the element shape function $[N_e]$ may be the same, because the corresponding DOFs of the non-zero terms in the two force vectors are different.

In a vehicle–bridge system, the relationship among the vertical displacement of vehicle body d_v , bridge deflection at the contact point $d_{b_contact}$, deformation of vehicle spring Δ_L , and road surface profile $r(x)$ can be expressed by the following equation:

$$\Delta_L = d_v - d_{b_contact} - r(x). \quad (15)$$

The first derivative of Eq. (15) can then be obtained as follows:

$$\dot{\Delta}_L = \dot{d}_v - \dot{d}_{b_contact} - \dot{r}(x) \quad (16)$$

where \dot{d}_v is the velocity of the vehicle body in the vertical direction; $\dot{r}(x) = \frac{dr(x)}{dx} \frac{dx}{dt} = \frac{dr(x)}{dx} V(t)$, where $V(t)$ is the vehicle traveling velocity; and $d_{b_contact}$, according to the definition of the shape function of the bridge in Eq. (14), can be expressed as follows:

$$d_{b_contact} = [N_e] \cdot \{d_{b_nodal}\} = [N_b] \cdot \{d_b\}. \quad (17)$$

In a situation when N vehicles are present on a bridge, by substituting Eqs. (15)–(17) into Eq. (2) the interaction force acting on the i th vehicle is obtained as follows:

$$\begin{aligned} F_{v-b}^i &= -K_v^i \cdot \Delta_L^i - C_v^i \cdot \dot{\Delta}_L^i \\ &= -K_v^i \cdot (d_v^i - [N_b^i] \{d_b\} - r(x)^i) \\ &\quad - C_v^i \cdot \left(\dot{d}_v^i - \frac{d[N_b^i]}{dx} \frac{dx}{dt} \{d_b\} - [N_b^i] \{\dot{d}_b\} - \frac{dr(x)^i}{dx} V^i(t) \right) \end{aligned} \quad (18)$$

where $[N_b^i]$ is the shape function of the bridge for an interaction force between the i th vehicle and the bridge. The N interaction forces acting on the N vehicles can be expressed in a vector form as follows:

$$\begin{aligned} \{F_{v-b}^N\} &= \{F_{v-b}^1 \quad F_{v-b}^2 \cdots F_{v-b}^n\}^T \\ &= -[K_v^N] \{d_v\} + [K_{v-b}] \{d_b\} + \{F_{v-r}\} \\ &\quad - [C_v^N] \{\dot{d}_v\} + [K_{v-cb}] \{d_b\} + [C_{v-b}] \{\dot{d}_b\} + \{F_{v-cr}\} \end{aligned} \quad (19)$$

where $[M_v^N]$, $[K_v^N]$, and $[C_v^N]$ are the diagonal mass, stiffness, and damping matrices for N vehicles, respectively; $\{d_b\}$ and $\{\dot{d}_b\}$ have the same definitions as in Eq. (4); and $[K_{v-b}]$, $\{F_{v-r}\}$, $[K_{v-cb}]$, $[C_{v-b}]$, and $\{F_{v-cr}\}$ are defined respectively as:

$$\begin{aligned} [K_{v-b}] &= [K_v^N] \cdot \left[[N_b^1]^T \quad [N_b^2]^T \cdots [N_b^n]^T \right]^T; \\ \{F_{v-r}\} &= [K_v^N] \cdot [r(x)^1 \quad r(x)^2 \cdots r(x)^n]^T; \\ [K_{v-cb}] &= [C_v^N] \cdot \frac{d \left[V^1(t) \cdot [N_b^1]^T \quad V^2(t) \cdot [N_b^2]^T \cdots V^n(t) \cdot [N_b^n]^T \right]^T}{dx}; \\ [C_{v-b}] &= [C_v^N] \cdot \left[[N_b^1]^T \quad [N_b^2]^T \cdots [N_b^n]^T \right]^T; \\ \{F_{v-cr}\} &= [C_v^N] \cdot \left[\frac{dr(x)^1}{dx} V^1(t) \quad \frac{dr(x)^2}{dx} V^2(t) \cdots \frac{dr(x)^n}{dx} V^n(t) \right]^T. \end{aligned}$$

As discussed earlier, the interaction forces acting on the bridge, $\{F_{b-v}\}$, are the reaction forces of that acting on the vehicles, $\{F_{v-b}\}$. Therefore, the following relationship holds:

$$\{F_{b-v}\} = -\{F_{v-b}\}. \quad (20)$$

Substituting Eqs. (18) and (20) into Eq. (14), the transformed equivalent nodal forces due to the N interaction forces on the bridge can be obtained as follows:

$$\begin{aligned} \{F_b^{eq}\} &= \sum_{i=1}^N [N_b^i]^T \cdot (-F_{v-b}^i) \\ &= \sum_{i=1}^N [N_b^i]^T \cdot \left(K_v^i \cdot (d_v^i - [N_b^i] \{d_b\} - r(x)^i) \right. \\ &\quad \left. + C_v^i \cdot \left(\dot{d}_v^i - \frac{d[N_b^i]}{dx} \frac{dx}{dt} \{d_b\} - [N_b^i] \{\dot{d}_b\} - \frac{dr(x)^i}{dx} V^i(t) \right) \right) \\ &= [K_{b-v}] \{d_v\} - [K_{b-vb}] \{d_b\} - \{F_{b-r}\} + [C_{b-v}] \{\dot{d}_v\} \\ &\quad - [K_{b-cb}] \{d_b\} - [C_{b-b}] \{\dot{d}_b\} - \{F_{b-cr}\} \end{aligned} \quad (21)$$

where $[K_{b-v}]$, $[K_{b-vb}]$, $\{F_{b-r}\}$, $[C_{b-v}]$, $[K_{b-cb}]$, $[C_{b-b}]$, and $\{F_{b-cr}\}$ are defined as follows:

$$[K_{b-v}] = \{ [N_b^1]^T \cdot K_v^1 \quad [N_b^2]^T \cdot K_v^2 \cdots [N_b^n]^T \cdot K_v^n \};$$

$$\begin{aligned}
[K_{b-vb}] &= \sum_{i=1}^n [N_b^i]^T \cdot K_v^i \cdot [N_b^i]; \\
\{F_{b-r}\} &= \sum_{i=1}^n [N_b^i]^T \cdot K_v^i \cdot r(x)^i; \\
[C_{b-v}] &= \{[N_b^1]^T \cdot C_v^1 \quad [N_b^2]^T \cdot C_v^2 \cdots [N_b^n]^T \cdot C_v^n\}; \\
[K_{b-cb}] &= \sum_{i=1}^n [N_b^i]^T \cdot C_v^i \cdot \frac{d[N_b^i]}{dx} V^i(t); \\
[C_{b-b}] &= \sum_{i=1}^n [N_b^i]^T \cdot C_v^i \cdot [N_b^i]; \\
\{F_{b-cr}\} &= \sum_{i=1}^n [N_b^i]^T \cdot C_v^i \cdot \left(\frac{dr(x)^i}{dx} V^i(t) \right).
\end{aligned}$$

Substituting Eq. (19) into Eq. (3), we have the following for vehicles:

$$\begin{aligned}
[M_v^N] \{\ddot{d}_v\} &= -F_G^N - [K_v^N] \{d_v\} + [K_{v-b}] \{d_b\} + \{F_{v-r}\} \\
&\quad - [C_v^N] \{\dot{d}_v\} + [K_{v-cb}] \{d_b\} + [C_{v-b}] \{\dot{d}_b\} + \{F_{v-cr}\}. \quad (22)
\end{aligned}$$

Since $\{F_b^{eq}\}$ in Eq. (21) is actually the equivalent force vector of the external force vector $\{F_b\}$ in Eq. (4), after substituting Eq. (21) into Eq. (4), the following can be obtained for the bridge:

$$\begin{aligned}
[M_b] \{\ddot{d}_b\} + [C_b] \{\dot{d}_b\} + [K_b] \{d_b\} \\
= [K_{b-v}] \{d_v\} - [K_{b-vb}] \{d_b\} - \{F_{b-r}\} + [C_{b-v}] \{\dot{d}_v\} \\
- [K_{b-cb}] \{d_b\} - [C_{b-b}] \{\dot{d}_b\} - \{F_{b-cr}\}. \quad (23)
\end{aligned}$$

Eqs. (22) and (23) can be combined to form a vehicle–bridge coupled system and rewritten in matrix form as below:

$$\begin{aligned}
\begin{bmatrix} M_b & \\ & M_v^N \end{bmatrix} \begin{Bmatrix} \ddot{d}_b \\ \ddot{d}_v \end{Bmatrix} + \begin{bmatrix} C_b + C_{b-b} & -C_{b-v} \\ -C_{v-b} & C_v^N \end{bmatrix} \begin{Bmatrix} \dot{d}_b \\ \dot{d}_v \end{Bmatrix} \\
+ \begin{bmatrix} K_b + K_{b-vb} + K_{b-cb} & -K_{b-v} \\ -K_{v-b} - K_{v-cb} & K_v^N \end{bmatrix} \begin{Bmatrix} d_b \\ d_v \end{Bmatrix} \\
= \begin{Bmatrix} -F_{b-r} - F_{b-cr} \\ F_{v-r} + F_{v-cr} - F_G^N \end{Bmatrix}. \quad (24)
\end{aligned}$$

Compared to Eqs. (3) and (4), there are additional terms, $C_{b-b}, C_{b-v}, C_{v-b}, K_{b-vb}, K_{b-cb}, K_{b-v}, K_{v-b}, K_{v-cb}, F_{b-r}, F_{b-cr}, F_{v-r}$, and F_{v-cr} in Eq. (24), which result due to the coupling effect between the bridge and vehicles. When a vehicle travels on the bridge, the position of the contact point changes with time, which means the road roughness $r(x)$ at the contact point and the shape function $[N_b]$ are both time-dependent terms, indicating that all the additional terms in Eq. (24) are time-dependent terms.

Using Eq. (8), Eq. (24) can be further rewritten as follows:

$$\begin{aligned}
\begin{bmatrix} I & \\ & M_v \end{bmatrix} \begin{Bmatrix} \ddot{\xi}_b \\ \dot{d}_v \end{Bmatrix} + \begin{bmatrix} 2\omega_i \eta_i I + \Phi_b^T C_{b-b} \Phi_b & -\Phi_b^T C_{b-v} \\ -C_{v-b} \Phi_b & C_v^N \end{bmatrix} \begin{Bmatrix} \dot{\xi}_b \\ \dot{d}_v \end{Bmatrix} \\
+ \begin{bmatrix} \omega_i^2 I + \Phi_b^T (K_{b-vb} + K_{b-cb}) \Phi_b & -\Phi_b^T K_{b-v} \\ -(K_{v-b} + K_{v-cb}) \Phi_b & K_v^N \end{bmatrix} \begin{Bmatrix} \xi_b \\ d_v \end{Bmatrix} \\
= \begin{Bmatrix} -\Phi_b^T (F_{b-r} + F_{b-cr}) \\ F_{v-r} + F_{v-cr} - F_G^N \end{Bmatrix} \quad (25)
\end{aligned}$$

where the vehicle–bridge coupled system contains only the modal properties of the bridge and the physical parameters of the vehicles.

Eq. (25) can be solved by the Runge–Kutta method in time domain. At each time step, the interaction force at each contact point is first calculated using Eq. (18). If it is negative, which means the corresponding vehicle leaves the road surface, then it should

be set to zero and the corresponding time-dependent terms in Eq. (25) should be modified. In such a way, this model can account for the situation when vehicles lose contact with the road surface. The solution to this system contains the interaction forces, physical displacement, velocity, and acceleration of the vehicles as well as the displacement, velocity, and acceleration of the bridge in the modal coordinates at each time step. The physical displacement, velocity, and acceleration of each node on the bridge can then be transformed from the modal coordinates using Eqs. (5)–(7). The strain (not directly solved in the MATLAB program) at any node i of the bridge in the longitudinal direction can also be estimated based on the average strain between the node of interest and its two adjacent nodes in the longitudinal direction, and was calculated using the expression below:

$$\varepsilon(i, t) = \frac{\frac{d_{i+1}(t) - d_i(t)}{L} + \frac{d_i(t) - d_{i-1}(t)}{L}}{2} = \frac{d_{i+1}(t) - d_{i-1}(t)}{2L} \quad (26)$$

where L represents the distance between two adjacent nodes in the longitudinal direction and $d_{i-1}(t)$, $d_i(t)$, and $d_{i+1}(t)$ denote the displacements of three consecutive nodes in the longitudinal direction, respectively. The strain information will be used later for the identification of vehicle axle loads.

Based on the above methodology, a MATLAB program named BIRDS-BVI (laboratory of Bridge Innovative Research and Dynamics of Structures – Bridge Vehicle Interaction) was developed to assemble the motion equations of the vehicle–bridge coupled system and to solve the coupling equations. The modal information of the bridge can be solved using any finite element program (such as ANSYS) and then imported to the MATLAB environment before assembling the equations.

3. Parameter identification using Genetic Algorithm

The problem of identifying parameters of vehicles traveling on bridges is actually an inverse optimization problem. In order to obtain the optimal parameters, a good searching tool is needed. In the present study the Genetic Algorithm was used.

Genetic algorithms [22,23] are stochastic global search techniques based on the mechanics of natural genetics. They have been widely applied in bioinformatics, phylogenetics, computer science, engineering, economics, chemistry, manufacturing, mathematics, physics, and other fields. GAs are implemented to an optimization problem as a computer simulation in which a population of abstract representations (usually called chromosomes) of candidate solutions (usually called individuals, creatures, or phenotypes) evolves toward better solutions. The evolution usually starts from a population of randomly generated individuals and continues in new generations. In each generation the fitness of every individual in the population is evaluated, multiple individuals are stochastically selected from the current population based on their fitness, and the population is modified to form a new population. The new population is then used in the next iteration of the algorithm. By doing this, the best genes of each generation are reserved and delivered to the next generations, and eventually the best gene or optimal solution is found.

To use the GA in the identification process, first an objective function based on the residual between the measured and simulated bridge response is built using the Least-Squares method, which is shown below:

$$F_{obj} = \sqrt{\sum_{i=1}^n (r_m(i) - r_s(i))^2} \quad (27)$$

where i and n are the time-point number and total number of time points in the response time history, respectively, and r_m and r_s are the measured and simulated response time histories, respectively.

After setting proper upper and lower bounds as well as a proper set of initial values for the parameters to be identified in the GA program, the objective function in Eq. (27) can then be optimized. It should be noted that since the GA is a global searching technique, the setting of the two bounds and initial values will not affect the accuracy of the final identified results for the parameters as long as the optimal values are within the bounds. However, a reasonable set of the two bounds and proper initial values can facilitate the identification process [22]. In an ideal case, the bounds should be large enough to include the optimal values but also small enough for computation efficiency. In general, the true optimal values are not known in advance and large conservative bounds can be set. In the present simulation, the lower and upper bounds were set to be 10% and 10 times the true values of the parameters, respectively, and the initial values of the parameters were set to be one-third of their true values. In identifying the parameters of the full-scale vehicle model the objective function may sometimes not achieve a pre-set satisfactory level after the optimization comes to the end. In these cases a multi-stage optimization strategy was used by setting the initial values for the next stage equal to the optimized results obtained at the current stage while keeping everything else unchanged.

The identification error was defined as the absolute percentage difference shown below:

$$\text{Identification error} = \left| \frac{P_{iden} - P_{true}}{P_{true}} \right| \times 100\% \quad (28)$$

where P_{iden} and P_{true} are the identified parameter and the true parameter, respectively.

4. Numerical simulations

To study the accuracy and efficiency of the proposed identification method, numerical simulations were carried out and a series of comprehensive case studies were conducted. The SDOF vehicle model was used in most simulation studies for the purpose of simplicity. The full-scale vehicle model, which will be used later to model a real truck used for field testing, was also examined. Bridge responses including displacement, acceleration, and strain were all used in the identification process. The effects of different factors, such as the number of modes used for the bridge model, vehicle speeds, traveling routes, number of vehicles, measurement stations, road surface conditions, and levels of measurement noise, were all examined.

A concrete slab bridge simply supported at both ends was used for all case studies. The bridge has a length of 12 m, a width of 8 m, and a depth of 0.3 m. This bridge was modeled using solid elements (with three translational DOFs for each node) with the ANSYS program (Fig. 2). The density, modulus of elasticity, and Poisson's ratio of the concrete were 2300 kg/m^3 , 210 GPa , and 0.15 , respectively. The parameters of all the vehicles used in this study were taken as follows: $m_v = 5 \times 10^3 \text{ kg}$; $k_v = 1.0 \times 10^6 \text{ N/m}$; and $c_v = 5.0 \times 10^2 \text{ Ns/m}$. The speed of the vehicle was set to 10 m/s in all cases except those studying the effect of different vehicle speeds. The time step was taken as 0.001 s , based on a preliminary sensitivity study.

In the present study a total of 9 measurement stations were originally selected from the bridge (Fig. 2). Because of the symmetry among the 9 measurement stations selected, only 4 of them (S1, S2, S4, and S5) were studied; those positions are listed in Table 1. Sensors were installed at the bottom of the bridge deck. Four traveling routes, R1, R2, R3, and R4, were used in this study, with lateral positions of $Y_1 = 1 \text{ m}$, $Y_2 = 2 \text{ m}$, $Y_3 = 4 \text{ m}$, and $Y_4 = 6 \text{ m}$, respectively, as indicated in Fig. 2. Errors of the identified results for all four case studies are summarized in Table 2 and will be discussed separately later.

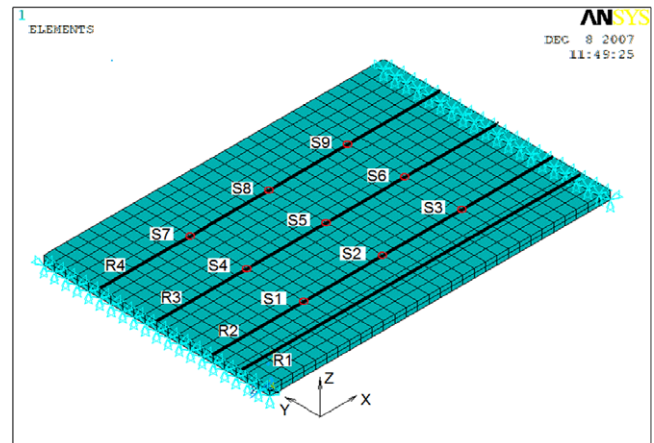


Fig. 2. The concrete slab bridge under study.

Table 1
Positions of measurement stations.

| Measurement Station | X (m) | Y (m) |
|---------------------|-------|-------|
| S1 | 3.2 | 2.0 |
| S2 | 6.0 | 2.0 |
| S4 | 3.2 | 4.0 |
| S5 | 6.0 | 4.0 |

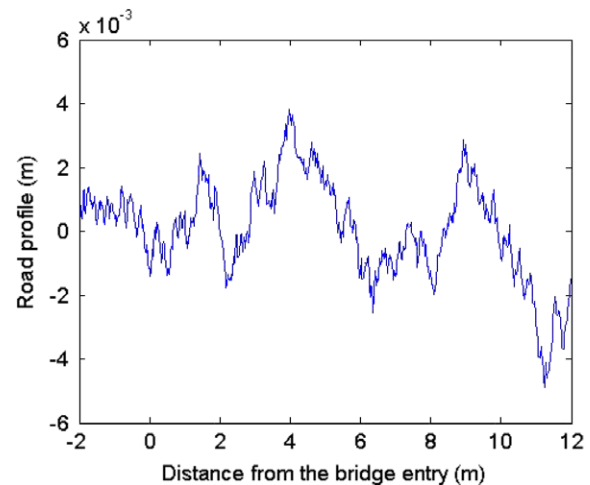


Fig. 3. A road surface profile (classified as good condition) used in the present study.

The same road surface profile (Fig. 3), which belongs to a good road surface condition based on the [21], was used for all of the case studies except the one in which the effect of different road surface conditions was studied.

4.1. Effect of number of modes

Since the modal superposition technique was used in constructing the bridge model in the present study, the number of modes used for the bridge model would have an impact on the dynamic response of the bridge. As a result, the identified results for the vehicle parameters would be affected by the number of modes used. It is known that high-frequency modes usually have less impact on a bridge response than low-frequency modes; therefore, it would be interesting to find out how many modes would be required to accurately identify the vehicle parameters.

In this paper it was assumed that in simulation 50 modes are able to produce accurate bridge responses, which can then be treated as true bridge responses for the purpose of comparison. Three cases with 5, 10, and 20 modes, respectively, were studied.

Table 2
Effect of different number of modes used for the bridge model.

| Number of modes | Bridge response used | Identified values | | | Errors | | |
|-----------------|----------------------|-------------------|-------------|----------|--------|--------|---------|
| | | M (kg) | K (1e6 N/m) | C (Ns/m) | M (%) | K (%) | C (%) |
| 5 | Deflection | 4932.3 | 0.955920 | 2158.20 | 1.354 | 4.408 | 331.640 |
| | Acceleration | 5072 | 0.958752 | 548.32 | 1.440 | 4.125 | 9.664 |
| | Strain | 5029.2 | 1.786960 | 50 | 0.584 | 78.696 | 90.000 |
| 10 | Deflection | 4972.9 | 1.001400 | 50 | 0.542 | 0.140 | 90.000 |
| | Acceleration | 5304 | 0.975136 | 817.62 | 6.080 | 2.486 | 63.524 |
| | Strain | 4925 | 1.559400 | 50 | 1.500 | 55.940 | 90.000 |
| 20 | Deflection | 4998 | 1.009440 | 671 | 0.040 | 0.944 | 34.200 |
| | Acceleration | 5000 | 1.000020 | 499.98 | 0.000 | 0.002 | 0.004 |
| | Strain | 4986 | 0.984624 | 982 | 0.280 | 1.538 | 96.400 |

It is noted that depending on the location of the vehicle, different modes can be excited, and some modes will be more dominant than the others. Therefore, the total number of modes is not enough to determine which modes should be used in the identification. As a matter of fact, it is difficult to determine in advance which modes should be used in the identification. Here the effect of mode number is investigated in a generic way by varying the total number of modes. In all three cases, the vehicle was traveling along route R2 at a constant speed of 10 m/s. The identified vehicle parameters and errors, based on deflection, acceleration, and strain, respectively, are shown in Table 2.

It can be seen from Table 2 that using 5 or 10 modes for the bridge model is obviously not enough since large errors exist for both the identified stiffness and damping under these two cases. Using 20 modes gives good results for the mass and stiffness with errors less than 2%; however, the error corresponding to the identified damping still reaches 96%. This large error could be attributed to the fact that the bridge responses are not sensitive to the change in vehicle damping, i.e., even a large change in vehicle damping will produce only a slight difference in the bridge response. As a result, a small difference in the bridge response, due to the different number of modes used or other reasons, could produce a large error in the identified damping, which will also be seen from the results of a sensitivity study of different vehicle parameters later.

For clarity it is noted that in the following simulations, unless stated otherwise, the simulated response from using 50 modes and the true vehicle parameters specified earlier are treated as true values. The other results from using also 50 modes and the vehicle parameters within the lower and upper bounds discussed earlier are treated as simulated values. By matching the simulated and true values, the vehicle parameters are identified through the GA.

4.2. Effect of different measurement stations

In bridge field testing, it is usually very important to choose the right position for the measurement station. The results from another study by the writers [24] when using influence surface method show that the position of the measurement station plays a crucial role in the dynamic axle load identification process. Placing the measurement station at the center of the bridge yielded the best results in their study. In this paper four measurement stations (S1, S2, S3, and S4) were selected and studied; their positions are shown in Table 1. The identified vehicle parameters and their errors are shown in Table 3.

It can be seen from the table that the position of the measurement station has an insignificant effect on the accuracy of the identified results. However, it should be noted that there is always noise in practice. The noise-to-signal ratio is usually higher near the supports or modal nodes than at the mid-span. In this case, measurement stations at the center of the bridge or away from nodes may yield the best results.

4.3. Effect of different vehicle speeds

To account for vehicles traveling at different speeds, three levels of vehicle speed were studied, namely 5 m/s, 10 m/s, and 20 m/s. In all three cases, the vehicle was traveling along route R2 at a constant speed. The bridge responses from S5 were used in the identification process. The identified vehicle parameters and their errors are shown in Table 4. As can be seen from the table, the vehicle speed has almost no effect on the identified results, indicating that the developed methodology can be used for routine traffic conditions. In comparison, most weigh-in-motion facilities do not work well for normal traveling vehicles and are only reliable for slow moving traffic.

4.4. Effect of different traveling routes

Vehicles can travel on a bridge in different lanes. In the present study the effects of a vehicle traveling along three different routes (R1, R2, and R3 as indicated in Fig. 2) were studied. The identified results are shown in Table 5. The results indicate that the identified results are not affected by the route along which the vehicle is traveling on the bridge, which, again, indicates the applicability of the developed methodology for actual, routine traffic conditions.

4.5. Effect of number of vehicles

Usually more than one vehicle is traveling on a bridge at the same time. To verify the proposed method for this situation, two case studies were carried out. In the first case, two vehicles were traveling along the same route (R1), one in front of the other, at a distance of 4 m. In the second case, three vehicles were traveling along two different routes (R1 and R4), namely two vehicles travel side by side along R1 and R4, and the third one travels along R1 4 m in front of them. The identified vehicle parameters and corresponding errors for these two cases are shown in Tables 6 and 7. As can be seen from the two tables, the proposed method works well for the multiple-vehicle situation.

4.6. Effect of different vehicle models

Different vehicle models have been used in the literature. In the present study a full-scale two-axle vehicle model shown in Fig. 4, which is the model of the test truck used in the field testing later, was also used in the simulation study, in addition to the SDOF model discussed earlier. This two-axle vehicle model was used by [18] as well as the writers in another study [25] to simulate a dump truck in a bridge field test. This model will also be used later in the field testing part of this paper. According to the study of [18], the following parameters were used for this vehicle in the present study. However, it is noted that only the dimensions, axle loads, and total weight of the vehicle were actually measured and are reliable information. The other information including stiffness, damping, etc. were not available and was assumed.

Table 3
Effect of different measurement stations.

| Measurement station | Bridge response used | Identified values | | | Errors | | |
|---------------------|----------------------|-------------------|-------------|----------|--------|-------|-------|
| | | M (kg) | K (1e6 N/m) | C (Ns/m) | M (%) | K (%) | C (%) |
| S1 | Deflection | 5000 | 0.999996 | 499.971 | 0 | 0.000 | 0.006 |
| | Acceleration | 5000 | 0.999999 | 500.024 | 0 | 0.000 | 0.005 |
| | Strain | 5000 | 1.000000 | 500.003 | 0 | 0.000 | 0.001 |
| S2 | Deflection | 5000 | 1.000003 | 499.955 | 0 | 0.000 | 0.009 |
| | Acceleration | 5000 | 1.000004 | 499.993 | 0 | 0.000 | 0.001 |
| | Strain | 5000 | 1.000003 | 499.986 | 0 | 0.000 | 0.003 |
| S4 | Deflection | 5000 | 1.000002 | 500.027 | 0 | 0.000 | 0.005 |
| | Acceleration | 5000 | 1.000000 | 500.014 | 0 | 0.000 | 0.003 |
| | Strain | 5000 | 1.000003 | 500.002 | 0 | 0.000 | 0.000 |
| S5 | Deflection | 5000 | 0.999999 | 500.012 | 0 | 0.000 | 0.002 |
| | Acceleration | 5000 | 0.999996 | 500.000 | 0 | 0.000 | 0.000 |
| | Strain | 5000 | 1.000004 | 499.957 | 0 | 0.000 | 0.009 |

Table 4
Effect of different vehicle speeds.

| Vehicle speed (m/s) | Bridge response used | Identified values | | | Errors | | |
|---------------------|----------------------|-------------------|-------------|----------|--------|-------|-------|
| | | M (kg) | K (1e6 N/m) | C (Ns/m) | M (%) | K (%) | C (%) |
| 5 | Deflection | 5000 | 1.000004 | 500.015 | 0 | 0.000 | 0.003 |
| | Acceleration | 5000 | 1.000004 | 499.994 | 0 | 0.000 | 0.001 |
| | Strain | 5000 | 0.999995 | 500.039 | 0 | 0.000 | 0.008 |
| 10 | Deflection | 5000 | 1.000000 | 499.981 | 0 | 0.000 | 0.004 |
| | Acceleration | 5000 | 0.999996 | 499.977 | 0 | 0.000 | 0.005 |
| | Strain | 5000 | 1.000003 | 500.038 | 0 | 0.000 | 0.008 |
| 20 | Deflection | 5000 | 0.999997 | 499.969 | 0 | 0.000 | 0.006 |
| | Acceleration | 5000 | 1.000003 | 500.015 | 0 | 0.000 | 0.003 |
| | Strain | 5000 | 1.000002 | 500.018 | 0 | 0.000 | 0.004 |

Table 5
Effect of different traveling routes.

| Traveling route | Bridge response used | Identified values | | | Errors | | |
|-----------------|----------------------|-------------------|-------------|----------|--------|-------|-------|
| | | M (kg) | K (1e6 N/m) | C (Ns/m) | M (%) | K (%) | C (%) |
| R1 | Deflection | 5000 | 1.000001 | 499.996 | 0 | 0.000 | 0.001 |
| | Acceleration | 5000 | 1.000002 | 499.967 | 0 | 0.000 | 0.007 |
| | Strain | 5000 | 1.000002 | 500.006 | 0 | 0.000 | 0.001 |
| R2 | Deflection | 5000 | 0.999998 | 499.988 | 0 | 0.000 | 0.002 |
| | Acceleration | 5000 | 0.999999 | 500.036 | 0 | 0.000 | 0.007 |
| | Strain | 5000 | 0.999997 | 499.953 | 0 | 0.000 | 0.009 |
| R3 | Deflection | 5000 | 1.000001 | 500.023 | 0 | 0.000 | 0.005 |
| | Acceleration | 5000 | 1.000000 | 499.951 | 0 | 0.000 | 0.010 |
| | Strain | 5000 | 1.000004 | 499.992 | 0 | 0.000 | 0.002 |

Table 6
Identified results for the two-vehicle situation.

| Bridge response used | Deflection | | Acceleration | | Strain | |
|----------------------|------------------|-----------|------------------|-----------|------------------|-----------|
| | Identified value | Error (%) | Identified value | Error (%) | Identified value | Error (%) |
| M1 (kg) | 4999.62 | 0.008 | 5000.40 | 0.008 | 4999.60 | 0.008 |
| K1 (1e6 N/m) | 0.999664 | 0.034 | 0.999695 | 0.031 | 1.000463 | 0.046 |
| C1 (Ns/m) | 500.444 | 0.089 | 499.599 | 0.080 | 500.389 | 0.078 |
| M2 (kg) | 5000.44 | 0.009 | 5000.08 | 0.002 | 4999.85 | 0.003 |
| K2 (1e6 N/m) | 0.999907 | 0.009 | 1.000420 | 0.042 | 0.999877 | 0.012 |
| C2 (Ns/m) | 499.920 | 0.016 | 500.294 | 0.059 | 500.142 | 0.028 |

Table 7
Identified results for the three-vehicle situation.

| Bridge response used | Deflection | | Acceleration | | Strain | |
|----------------------|------------------|-----------|------------------|-----------|------------------|-----------|
| | Identified value | Error (%) | Identified value | Error (%) | Identified value | Error (%) |
| M1 (kg) | 5000.74 | 0.015 | 4995.03 | 0.099 | 5001.53 | 0.031 |
| K1 (1e6 N/m) | 0.997111 | 0.289 | 0.996975 | 0.302 | 1.002250 | 0.225 |
| C1 (Ns/m) | 497.218 | 0.556 | 490.037 | 1.993 | 503.962 | 0.792 |
| M2 (kg) | 5003.19 | 0.064 | 5000.42 | 0.008 | 4998.85 | 0.023 |
| K2 (1e6 N/m) | 1.000418 | 0.042 | 0.997080 | 0.292 | 1.001549 | 0.155 |
| C2 (Ns/m) | 497.999 | 0.400 | 498.652 | 0.270 | 492.345 | 1.531 |
| M3 (kg) | 4996.01 | 0.080 | 4995.10 | 0.098 | 5001.11 | 0.022 |
| K3 (1e6 N/m) | 1.001289 | 0.129 | 0.996000 | 0.400 | 0.998371 | 0.163 |
| C3 (Ns/m) | 492.741 | 1.452 | 497.877 | 0.425 | 499.146 | 0.171 |

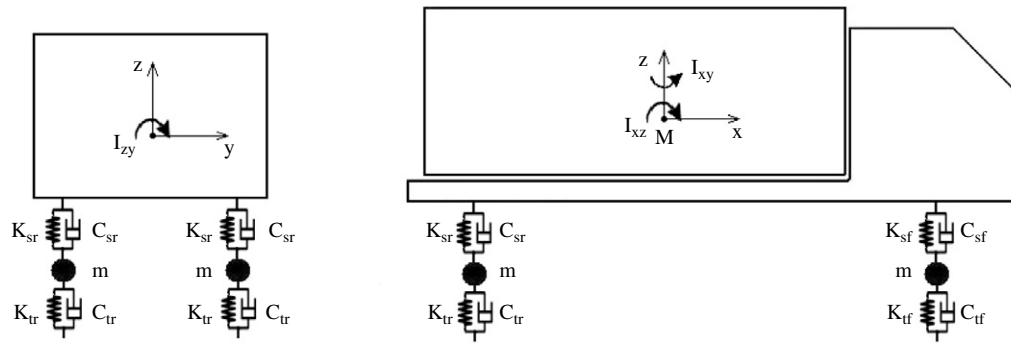


Fig. 4. A full-scale 2-axle vehicle model.

Table 8

Identified results for the parameters of the full-scale vehicle model.

| Bridge Response used | Acceleration | | | Displacement | | Strain | |
|--|--------------|------------------|-----------|------------------|-----------|------------------|-----------|
| Parameter | True value | Identified value | Error (%) | Identified value | Error (%) | Identified value | Error (%) |
| M (kg) | 24,808 | 4,805 | 0.01 | 24,807 | 0.00 | 24,801 | 0.03 |
| I_{xy}, I_{xz} (kg. m ²) | 172,160 | 169,691 | 1.43 | 172,198 | 0.02 | 172,276 | 0.07 |
| I_{zy} (kg. m ²) | 31,496 | 31,269 | 0.72 | 31,524 | 0.09 | 31,531 | 0.11 |
| m (kg) | 725.4 | 722.1 | 0.45 | 725.8 | 0.06 | 726.75 | 0.19 |
| K_{sf} (N/m) | 727,812 | 720,040 | 1.07 | 728,144 | 0.05 | 728,658 | 0.12 |
| K_{sr} (N/m) | 1969,034 | 1950,932 | 0.92 | 1968,820 | 0.01 | 1968,864 | 0.01 |
| C_{sf} (Ns/m) | 2189.6 | 2178.7 | 0.50 | 2190.8 | 0.05 | 2188.7 | 0.04 |
| C_{sr} (Ns/m) | 7181.8 | 7143.9 | 0.53 | 7190 | 0.11 | 7192 | 0.14 |
| K_{tf} (N/m) | 1972,900 | 1968,606 | 0.22 | 1973,576 | 0.03 | 1977,688 | 0.24 |
| K_{tr} (N/m) | 4735,000 | 4725,564 | 0.20 | 4737,908 | 0.06 | 4740884 | 0.12 |

Mass of vehicle body:

$$M = 24,808 \text{ kg};$$

Moments of inertia of the vehicle body:

$$I_{xy} = I_{xz} = 172,160 \text{ kg. m}^2;$$

$$I_{zy} = 31,496 \text{ kg. m}^2;$$

Mass combination of tire and suspension system:

$$m = 725.4 \text{ kg};$$

Stiffness of the suspension systems:

$$\text{front axle : } K_{sf} = 727,812 \text{ N/m};$$

$$\text{rear axle : } K_{sr} = 1,969,034 \text{ N/m};$$

Damping of the suspension systems:

$$\text{front axle : } C_{sf} = 2,189.6 \text{ Ns/m};$$

$$\text{rear axle : } C_{sr} = 7,181.8 \text{ Ns/m};$$

Stiffness of the tires:

$$\text{front axle : } K_{tf} = 1,972,900 \text{ N/m};$$

$$\text{rear axle : } K_{tr} = 4,735,000 \text{ N/m};$$

Damping of the tires:

$$\text{front axle : } C_{tf} = 0 \text{ Ns/m};$$

$$\text{rear axle : } C_{tr} = 0 \text{ Ns/m}.$$

The bridge responses from S5 when the truck was traveling across the bridge at a speed of 10 m/s were used in the identification process. The parameters selected to be identified and their identified results obtained using the multi-stage optimization strategy are shown in Table 8.

As can be seen from the table, the parameters of the full-scale vehicle model have been successfully identified with good

accuracy. Using acceleration yields results of lower accuracy compared to using displacement and strain when the same number of stages was used (3 stages in this case); however, if more stages had been used in the multi-stage identification process, the results could have been further improved.

4.7. Effect of different road surface conditions

Three levels of road surface conditions were studied, namely good, average, and poor according to [21]. The identified parameters of the vehicle and the corresponding errors when using responses from S5 in the identification process are shown in Table 9. From the table it can be seen that the road surface condition has little effect on the identified results. Again, most weigh-in-motion facilities do not work well with rough surface conditions, which result in significant dynamic effects. It is noted that the road surface roughness has a large effect on the vibration of both bridges and vehicles, especially when the vehicles are moving at high speed. However, the identified vehicle parameters such as weight should not be affected by the road roughness, as demonstrated by the present methodology.

4.8. Effect of different noise levels

In the simulations discussed above, extremely accurate results were achieved in ideal situations. Since measurement noise always exists in real tests, the effect of measurement noise was investigated here, and the noise-polluted responses were used to identify the parameters. The noise-polluted response was simulated by adding to the original noise-free response, which is a vector, an additional noise vector. The root-mean-square value of the noise is equal to a certain percentage of that of the original noise-free response. All elements in the noise vector are uncorrelated and are of the Gaussian distribution with a zero mean and unit standard deviation. Three different levels of noise, namely

Table 9
Effect of different road surface conditions.

| Road surface condition | Bridge response | Identified values | | | Errors | | |
|------------------------|-----------------|-------------------|-------------|----------|--------|-------|-------|
| | | M (kg) | K (1e6 N/m) | C (Ns/m) | M (%) | K (%) | C (%) |
| Good | Deflection | 5000 | 0.999998 | 499.968 | 0 | 0.000 | 0.006 |
| | Acceleration | 5000 | 1.000002 | 500.019 | 0 | 0.000 | 0.004 |
| | Strain | 5000 | 0.999999 | 499.977 | 0 | 0.000 | 0.005 |
| Average | Deflection | 5000 | 1.000002 | 500.022 | 0 | 0.000 | 0.004 |
| | Acceleration | 5000 | 0.999999 | 500.021 | 0 | 0.000 | 0.004 |
| | Strain | 5000 | 0.999997 | 500.004 | 0 | 0.000 | 0.001 |
| Poor | Deflection | 5000 | 1.000004 | 499.973 | 0 | 0.000 | 0.005 |
| | Acceleration | 5000 | 0.999999 | 499.956 | 0 | 0.000 | 0.009 |
| | Strain | 5000 | 0.999998 | 499.975 | 0 | 0.000 | 0.005 |

Table 10
Effect of different noise levels.

| Noise level (%) | Bridge response | Identified values | | | Errors | | |
|-----------------|-----------------|-------------------|-------------|----------|--------|--------|---------|
| | | M (kg) | K (1e6 N/m) | C (Ns/m) | M (%) | K (%) | C (%) |
| 1 | Deflection | 4940 | 1.004064 | 804 | 1.200 | 0.406 | 60.800 |
| | Acceleration | 4947 | 0.988693 | 489 | 1.060 | 1.131 | 2.200 |
| | Strain | 4944 | 0.991520 | 1372 | 1.120 | 0.848 | 174.400 |
| 5 | Deflection | 4816 | 1.037856 | 815 | 3.680 | 3.786 | 63.000 |
| | Acceleration | 4803 | 0.955925 | 516 | 3.940 | 4.408 | 3.200 |
| | Strain | 4816 | 0.958752 | 1348 | 3.680 | 4.125 | 169.600 |
| 10 | Deflection | 4496 | 1.021472 | 1252 | 10.080 | 2.147 | 150.400 |
| | Acceleration | 4739 | 0.955925 | 455 | 5.220 | 4.408 | 9.000 |
| | Strain | 4560 | 0.893216 | 996 | 8.800 | 10.678 | 99.200 |

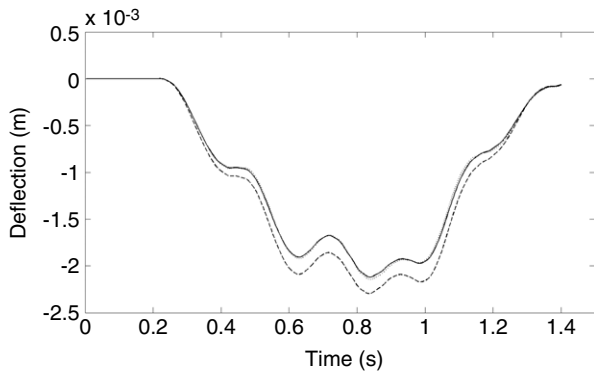


Fig. 5. Deflection time histories under a 10% change for each of the three parameters (—, no change for any parameter; ---, mass; ····, spring stiffness; - · - ·, damping).

1%, 5%, and 10%, were used in the present study. Identified vehicle parameters and their errors are shown in Table 10.

From the table it can be seen that the errors for the identified mass increases as the noise level increases, and the error reaches a maximum of 10% with a noise level of 10% when the deflection is used in the identification process. Similarly, the error for the identified spring stiffness reaches a maximum of 11% with a 10% noise level when strain is used in the identification process. However, the error accompanying the identified damping is significant even when the noise level is only 1%. A possible explanation for this large difference could be the fact that all three bridge responses are not sensitive to the change in vehicle damping, as discussed earlier.

Figs. 5–7 show the results of a sensitivity study of the three parameters, *M*, *K* and *C*. In each case, one parameter is increased by 10% while the other two are kept the same. From the figures we can see that very clear differences arise in the time histories of all three responses (deflection, acceleration, and strain) when the mass is increased by 10%. The differences can also be seen when the spring stiffness is increased by 10%; however, they are

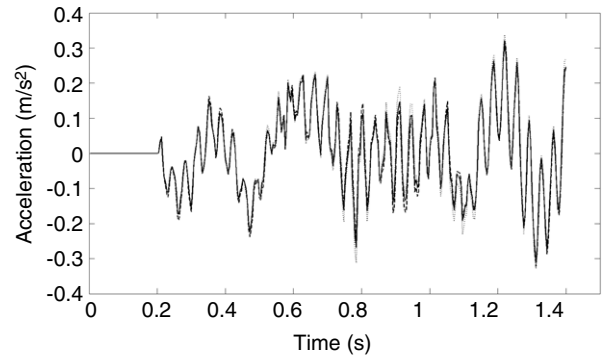


Fig. 6. Acceleration time histories under a 10% change for each of the three parameters (—, no change for any parameter; ---, mass; ····, spring stiffness; - · - ·, damping).

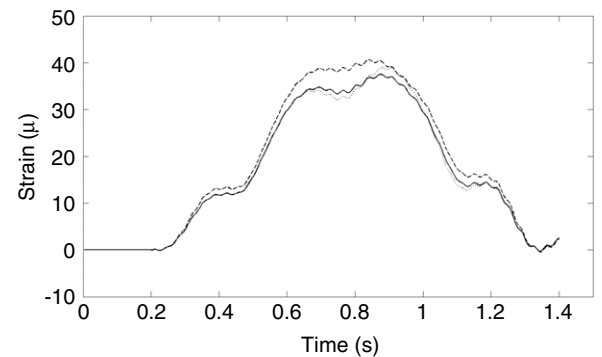


Fig. 7. Strain time histories under a 10% change for each of the three parameters (—, no change for any parameter; ---, mass; ····, spring stiffness; - · - ·, damping).

hardly detectable when the vehicle damping is increased by 10%. These results suggest that all three responses are not sensitive to the change in vehicle damping; and as a result, even a small disturbance in the responses could introduce a significant error in the identified result for the damping.

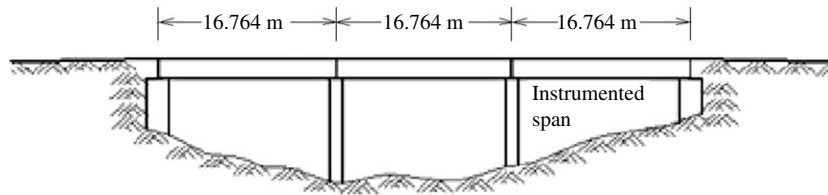


Fig. 8. Profile of the test bridge.

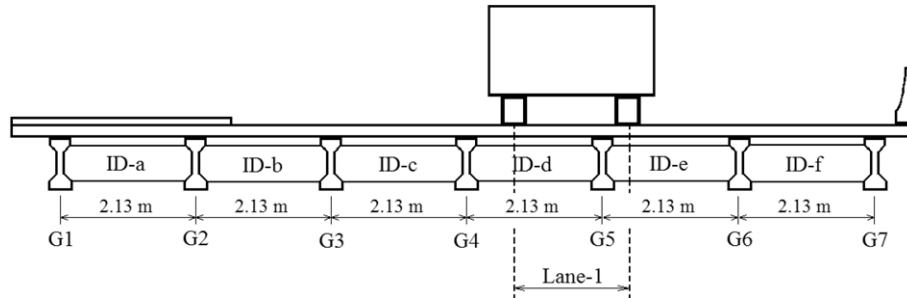


Fig. 9. Cross-section of the bridge and the position of Lane-1.

5. Field testing

5.1. Tested bridge

The tested bridge is located over Cypress Bayou in District 61, on LA 408 East, Louisiana. It has three straight simple spans, each measuring 16.764 m (55 ft) in length with zero skew angles (Fig. 8). As shown in Fig. 9, seven AASHTO Type II pre-stressed concrete girders spaced 2.13 m (7 ft) from center to center are used for the bridge. All girders are supported by rubber bearings at both ends. Each span has one intermediate diaphragm (ID) located at the mid-span as well as two more located at each end of the span, all of which are separated from the bridge deck.

The third span of the bridge was instrumented. A total of seven measurement stations (S1, S2, S3, S4, S5, S6, and S7 corresponding to girders G1, G2, G3, G4, G5, G6, and G7) were selected, each with a distance of 0.305 m (1 ft) from the mid-span of the corresponding girder to avoid stress concentration near the diaphragm. Strain gages, accelerometers, and cable extension transducers were placed at each of the seven stations.

Based on the configuration of the bridge, a FE bridge model was created using the ANSYS program (Fig. 10). The bridge deck, girders, diaphragms, shoulder, and railing were all modeled using solid elements, which have three translational degrees-of-freedom (DOF) for each node. The rubber bearings were modeled using equivalent beam elements with six DOFs (three translational and three rotational) for each node. Rigid connections were assumed between the rubber bearings and supports and also between the girders and diaphragms. Full composite actions were assumed between the girders and bridge deck.

The bridge model was updated by the writers in another study using the field measurements [26]. Five parameters including the Young's modulus for the bridge deck, seven girders, and diaphragms, respectively, the density of the bridge deck, and the equivalent Young's modulus for the rubber bearings were treated as variables with original values assumed to be 25.12 GPa, 32.03 GPa, 25.12 GPa, 2323 kg/m³, and 200 MPa, respectively. The five parameters were then updated with two different criteria depending on the purpose of model updating. With the purpose of achieving the best agreement possible between the measured natural frequencies and strains on the seven girders and their counterparts predicted by the FE bridge model, the following

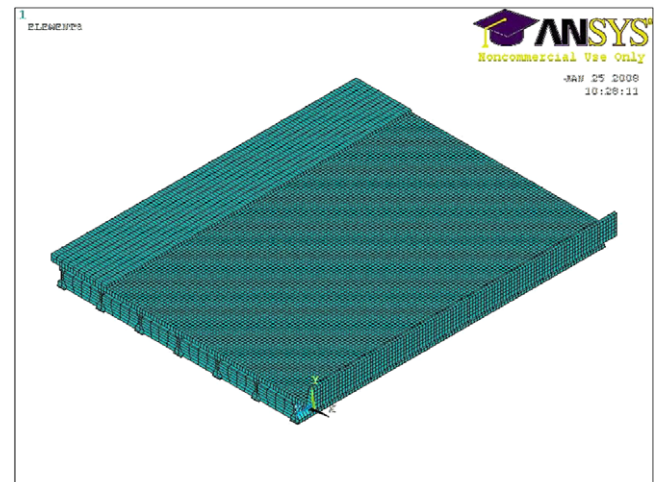


Fig. 10. Numerical model of the test bridge.

updated values for the five parameters were obtained: 29.44 GPa, 35.87 GPa, 10.07 GPa, 2693 kg/m³, and 53.5 MPa. The five parameters were also updated based on the natural frequencies and deflections of the seven girders, and the following updated results were obtained: 24.77 GPa, 27.67 GPa, 10.0 GPa, 2705 kg/m³, and 33.06 MPa, respectively.

Significant differences can be found between the two sets of updated parameters obtained with different purposes. One possible reason for the differences could be that the measured deflections were larger than the true deflections on the seven girders since the deflection gages were set on sand instead of on a solid base. An overestimated deflection makes the updated bridge model more flexible than it really was. However, as will be shown later, the total weight of the vehicle can be identified based on either strain or deflection, as long as the corresponding updated model is used in the identification process.

5.2. Test truck

The truck used in the bridge testing is a dump truck with a single front axle and a two-axle group for the rear (Fig. 11). The static loads for the first, second, and third axle of this truck are 80.0 kN,



Fig. 11. Dump truck used in bridge testing.

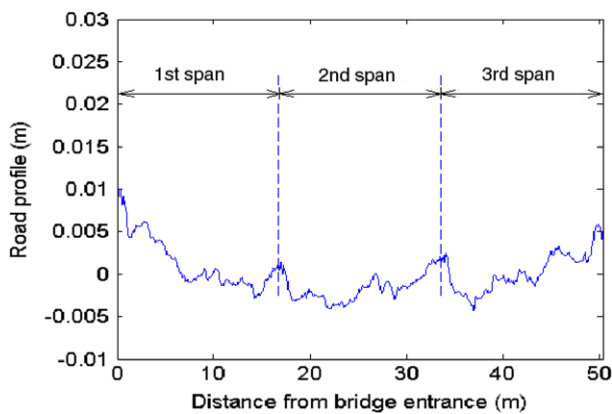


Fig. 12. Road surface profile along Lane-1.

95.6 kN, and 95.6 kN, respectively. The distance between the front axle and the center of the two rear axles is 6.25 m, and the distance between the two rear axles is 1.2 m.

Chan and O'Conner [27] conducted a detailed study on the dynamic effect caused by heavy vehicles, and they concluded that the two groups of axles can be replaced by one equivalent axle acting at the center of the two groups if the two groups of axles are close enough. To simplify the loading identification problem for the 3-axle truck, the two groups of axles at the rear of the truck were replaced by one equivalent axle in the present study, and the truck was modeled using a full-scale two-axle vehicle model shown in Fig. 4. This vehicle model is a combination of a rigid body connected to four masses by a series of springs and damping devices, with the rigid body representing the vehicle body and the linear elastic springs and dashpots representing the tires and suspension systems [18].

5.3. Road surface profile

The irregularity (roughness) of the bridge deck was measured by a laser profiler, which obtains the longitudinal road surface profile along each wheel track. For simplicity or due to the limitation of the vehicle–bridge model, in most previous studies two-dimensional road surface profiles were used [28,29,18] in which the change in road elevation along the lateral direction was not considered. A two-dimensional road surface profile is also used in this paper. Fig. 12 shows the measured road surface profile of Lane-1 along the track of the right wheel of the truck.

Since the finite element model was updated based on deflections or strains, there is a significant difference between the measured and simulated acceleration when the measured road surface profile is used in the simulation study [25]. Therefore, in the present study only the displacement and strain time histories

were used in the identification process. Table 11 shows the identified parameters and errors obtained using the full-scale vehicle model when displacement and strain are used.

As can be seen from the table, significant differences exist for all parameters except the mass of the vehicle body. As stated earlier, the true values except the mass in Table 11 are estimated values themselves and therefore they could differ significantly from their real values. These vehicle parameters are not available and difficult to measure, which actually provides a strong motivation for this study to identify them from field. Though we cannot judge directly the accuracy of the other identified parameters because we do not know their true values, the total mass of the truck could be used as a very important parameter to examine the accuracy of the identified results because the total weight of the test truck is available. The difference for the total mass of the truck is calculated and shown in the last row of Table 11. The results indicate that the errors in both cases are less than 4%, which is acceptable in practice. Of course, as discussed earlier, the accuracy of some parameters such as damping is very sensitive to measurement errors, or noise.

Another way to examine the accuracy of parameter identification is to reconstruct the bridge response using the identified parameters. As evidenced in Fig. 13, which shows the measured and reconstructed displacement and strain time histories at S4, respectively, a good match between the measured and reconstructed responses by using the identified truck parameters was achieved. Again, bridge displacements and strains are not sensitive to vehicle damping and one should be cautious when using these identified damping values.

6. Conclusions

A three-dimensional vehicle–bridge system has been developed taking into consideration the coupling effect between bridges and vehicles. The responses of bridges such as displacement, acceleration, and strain can be obtained by solving the vehicle–bridge coupling equations. The Genetic Algorithm has been used to identify the parameters of the vehicles traveling on bridges. Bridge responses including displacement, acceleration, and strain have all been used in the identification process. A series of comprehensive case studies, as well as field testing, have been carried out. Based on the results obtained from the case studies and field testing, the following conclusions can be drawn:

- (1) Bridge responses including displacement, acceleration, and strain can all be used to successfully identify the parameters of vehicles traveling on a bridge.
- (2) Factors such as measurement station, vehicle speed, traveling route, number of vehicles, vehicle model, and road surface condition have an insignificant effect on the identified vehicle parameters.
- (3) The number of modes used for the bridge model has a significant impact on the identified results; twenty modes are suggested in order to identify the vehicle mass and spring stiffness accurately based on the results from the simulation study. In order to identify the damping coefficient accurately, more modes are needed.
- (4) Noise has insignificant effect on the identified mass and spring stiffness of the vehicle; however, it has a significant impact on the identified damping coefficient because all three bridge responses are not sensitive to the change in the vehicle damping coefficient.
- (5) In order to successfully identify the vehicle parameters during field testing, an accurate vehicle–bridge model is needed, which is usually not possible in the real case. However, if the total weight is the only concern, good accuracy can be achieved when displacement or strain is used in the identification process.

Table 11
Identified parameters of the full-scale vehicle model from field testing.

| Response used | | Displacement | | Strain | |
|--|------------|------------------|-----------|------------------|-----------|
| Parameter | True value | Identified value | Error (%) | Identified value | Error (%) |
| M (kg) | 24,808 | 24,555 | 1.02 | 22,635 | 8.76 |
| I_{xy}, I_{xz} (kg. m ²) | 172,160 | 472,750 | 174.60 | 931,510 | 441.07 |
| I_{zy} (kg. m ²) | 31,496 | 56,283 | 78.70 | 77,856 | 147.19 |
| m (kg) | 725.4 | 523.00 | 27.90 | 1099 | 51.50 |
| K_{sf} (N/m) | 727,812 | 2,344,800 | 222.17 | 4,392,800 | 503.56 |
| K_{sr} (N/m) | 1969,034 | 3,103,000 | 57.59 | 8,313,100 | 322.19 |
| C_{sf} (Ns/m) | 2189.6 | 11,300 | 416.08 | 11,380 | 419.73 |
| C_{sr} (Ns/m) | 7181.8 | 48,659 | 577.53 | 7443.5 | 3.64 |
| K_{tf} (N/m) | 1972,900 | 2,094,600 | 6.17 | 5846,600 | 196.35 |
| K_{tr} (N/m) | 4735000 | 32,862,000 | 594.02 | 12,611,000 | 166.34 |
| Total Mass (kg) | 27,709.6 | 26,647 | 3.83 | 27,031 | 2.45 |

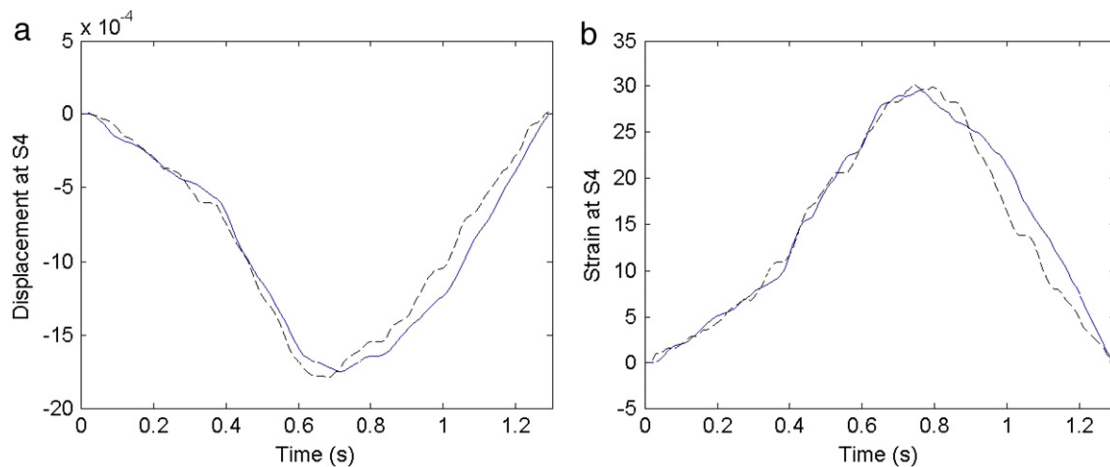


Fig. 13. Comparison of measured and reconstructed bridge responses (a) displacement; (b) strain time histories at S4 (— reconstructed; --- measured).

Since it is able to successfully identify the total weight of real vehicles, the proposed methodology can be applied to monitor routine traffic, which would be a significant advantage over the current weigh-in-motion techniques that usually require a smooth road surface and slow vehicle movement.

Acknowledgements

The field test is part of a project supported by Louisiana Transportation Research Center. The LADOTD crew helped conduct the bridge field test, and many graduate students and visiting scholars (M. Araujo, W. Wu, X. Shi., X. Liu, A. Nair, M. Xia, etc.) at the lab of Bridge Innovative Research and Dynamics of Structures, LSU also helped prepare and carry out the bridge test. These helps are appreciated.

References

- [1] Law SS, Chan THT, Zeng QH. Moving force identification: A time domains method. *J Sound Vib* 1997;201(1):1–22.
- [2] Law SS, Chan THT, Zeng QH. Moving force identification: A frequency and time domains analysis. *J Dyn Syst Meas Control* 1999;12(3):394–401.
- [3] Law SS, Chan THT, Zhu XQ, Zeng QH. Regularization in moving force identification. *J Eng Mech* 2001;127(2):136–48.
- [4] Zhu XQ, Law SS. Practical aspects in moving load identification. *J Sound Vib* 2002;258(1):123–46.
- [5] Chan THT, Ashebo DB. Theoretical study of moving force identification on continuous bridges. *J Sound Vib* 2006;295:870–83.
- [6] Au FTK, Jiang RJ, Cheung YK. Parameter identification of vehicles moving on continuous bridges. *J Sound Vib* 2004;269:91–111.
- [7] Jiang RJ, Au FTK, Cheung YK. Identification of vehicles moving on continuous bridges with rough surface. *J Sound Vib* 2004;274:1045–63.
- [8] Bu JQ, Law SS, Zhu XQ. Innovative bridge condition assessment from dynamic response of a passing vehicle. *J Eng Mech* 2006;132(12):1372–9.
- [9] Law SS, Bu JQ, Zhu XQ, Chan SL. Vehicle condition surveillance on continuous bridges on response sensitivity. *J Eng Mech* 2006;132(1):78–86.
- [10] Kyongsu Y, Hedrick K. Observer-based identification of nonlinear system parameters. *J Dyn Syst Meas Control* 1995;117(2):175–82.
- [11] Derradji DA, Mort N. Multivariable adaptive control using artificial neural networks. In: Proceedings of the 1996 UKACC international conference on control. Part 2 (of 2), vol. 427/2, 1996, p. 889–93.
- [12] Zheng DY, Cheung YK, Au FTK, Cheng YS. Vibration of multi-span non-uniform beams under moving loads by using modified beam vibration functions. *J Sound Vib* 1998;212(3):455–67.
- [13] Yu L, Chan THT. Recent research on identification of moving loads on bridges. *J Sound Vib* 2007;305:3–21.
- [14] Chatterjee PK, Datta TK, Surana CS. Vibration of suspension bridges under vehicular movement. *J Struct Eng* 1994;120(3):681–703.
- [15] Yang B, Tan CA, Bergman LA. Direct numerical procedure for solution of moving oscillator problems. *J Eng Mech* 2000;126(5):462–9.
- [16] Bilello LA, Bergman LA, Kuchma D. Experimental investigation of a small-scale bridge model under a moving mass. *J Struct Eng* 2004;130(5):799–804.
- [17] Shi XM, Cai CS, Chen SR. Vehicle induced dynamic behavior of short span bridges considering effect of approach span condition. *J Bridge Eng ASCE* 2008;13(1):83–92.
- [18] Shi XM. Structural performance of approach slab and its effect on vehicle induced bridge dynamic response. Ph.D. dissertation. Baton Rouge (LA): Louisiana State University; 2006.
- [19] Dodds CJ, Robson JD. The description of road surface roughness. *J Sound Vib* 1973;31(2):175–83.
- [20] Huang DZ, Wang TL. Impact analysis of cable-stayed bridges. *Comput Struct* 1992;43(5):897–908.
- [21] International Organization for Standardization (ISO). Mechanical vibration—road surface profiles—reporting of measured data. ISO 8068: 1995 (E), ISO. Geneva; 1995.
- [22] Goldberg DE. Genetic algorithms in search, optimization, and machine learning. Reading (MA, USA): Addison-Wesley Publishing Company, Inc.; 1989.
- [23] Gen M, Cheng R. Genetic algorithms & engineering design. New York (USA): John Wiley & Sons, Inc.; 1997.
- [24] Deng L, Cai CS. Identification of dynamic vehicular axle loads Part I: Theory and simulation studies. *J Vib Control* 2008 [submitted for publication].
- [25] Deng L, Cai CS. Identification of dynamic vehicular axle loads Part II: Field study. *J Vib Control* 2008 [submitted for publication].
- [26] Deng L, Cai CS. Bridge model updating using response surface method and genetic algorithm. *J Bridge Engineering, ASCE* [Accepted].
- [27] Chan THT, O'Conner C. Vehicle model for highway bridge impact. *J Struct Eng* 1990;116:1772–93.
- [28] Yang YB, Liao SS, Lin BH. Impact formulas for vehicles moving over simple and continuous beams. *J Struct Eng* 1995;121(11):1644–50.
- [29] Au FTK, Wang JJ, Cheung YK. Impact study of cable-stayed bridge under railway traffic using various models. *J Sound Vib* 2001;240(3):447–65.